Supporting Information

Self-gelation involved in transformation from co-amorphous system of resveratrol and piperine into a co-crystal system

Jiawei Han[‡ab], Luyuan Li[‡a], Qian Yu[‡a], Daoyi Zheng[c], Yutong Song[c], Jianjun Zhang[c], Yuan Gao[a], Weili Heng[a], Shuai Qian[*a], Zunting Pang[*a]

[a] School of Traditional Chinese Pharmacy, China Pharmaceutical University, Nanjing, 211198, P.R., China

[b] School of Pharmacy, Changzhou University, Changzhou, 213164, P.R., China

[c] School of Pharmacy, China Pharmaceutical University, Nanjing, 211198, P.R., China

---

[‡] These authors contributed equally to this work.

Corresponding authors and address for reprint:
[*] Corresponding authors
Dr. Shuai Qian
School of Traditional Chinese Pharmacy, China Pharmaceutical University, Nanjing,
Tel.: +86 139 1595 7175;
E-mail: silence_qs@163.com

Dr. Zunting Pang
School of Traditional Chinese Pharmacy, China Pharmaceutical University, Nanjing,
Tel.: +86 152 9577 1726;
E-mail: 15295771726@163.com

1 **Table S1** Comparisons between co-crystal and co-amorphous systems

| Items	Co-crystal system	Co-amorphous system
Solid form	Crystalline solid	Amorphous solid
Molecular packing	Periodic molecular arrangement	Long-range disorder molecular packing
Components	Binary or multi-components	
Co-former	Small molecules (excipients or drugs)	
Intermolecular interactions	Noncovalent interactions	Noncovalent interactions/No interaction
Stoichiometric ratio	A certain stoichiometric ratio	A certain stoichiometric ratio
Melting temperature (T_m)	A single T_m	N/A
Glass transition temperature (T_g)	N/A	A single T_g
Thermodynamics	Low-energy state	High-energy state
Solubility	Improvement (depending on the nature of co-former)	
Dissolution	Improvement (depending on the nature of co-former)	

2 N/A = not available.

3

1. Preparation of RES-PIP CM and RES-PIP CC
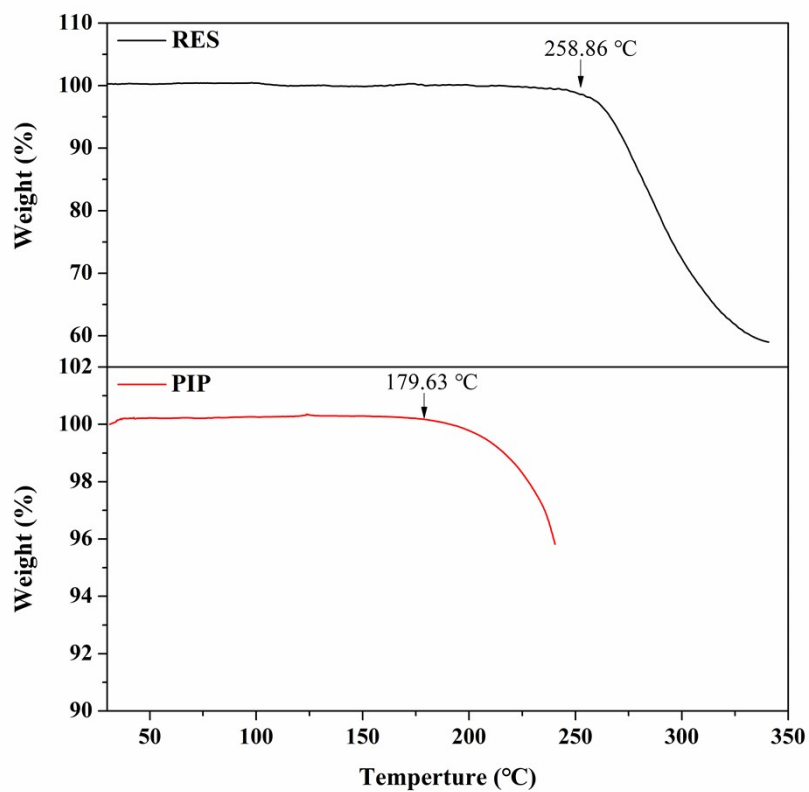
Fig. S1 TGA charts of crystalline RES and crystalline PIP.
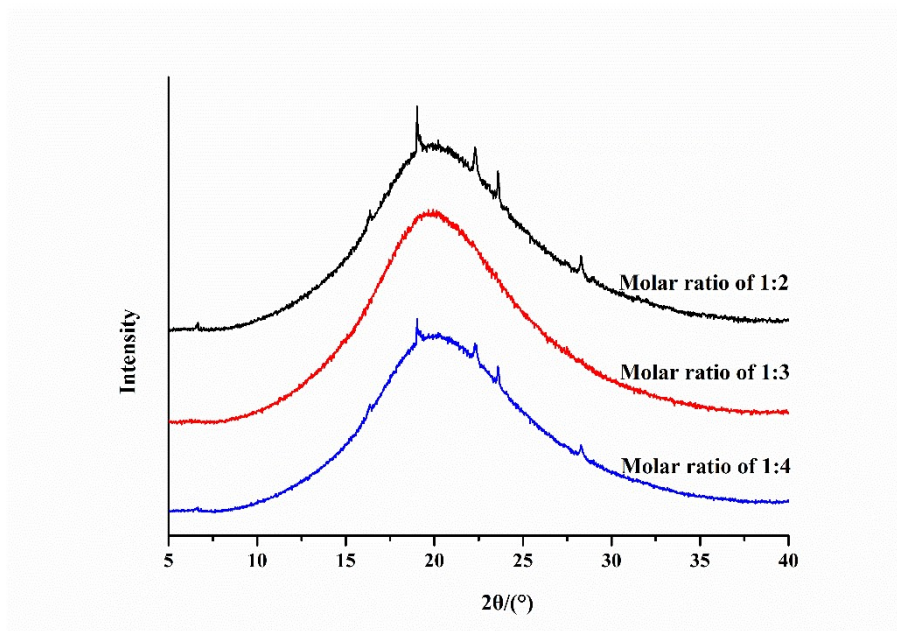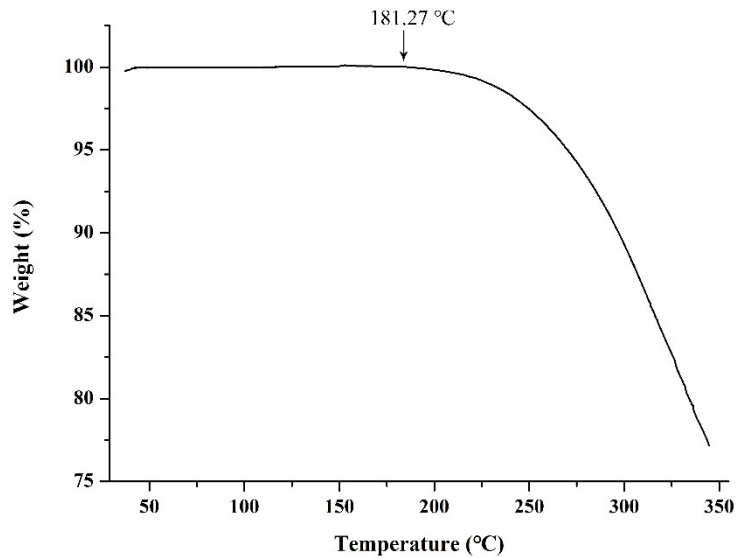

Fig. S2 XRPD diffractograms of the prepared product with molar ratios (RES/PIP) of 1:2, 1:3 and 1:4 by quench cooling.

10

11

12 **Fig. S3** TGA chart of RES-PIP CC.

13

14 **2. Determination of drug content in RES-PIP CM and RES-PIP CC**

15 The analysis was conducted on the LC-2010A HPLC analysis system (Shimadzu Co.,

16 Ltd., Tokyo, Japan) with an Ultimate C18 column (5 μm, 250 mm × 4.6 mm) at 35 °C.

17 The mobile phase (50:50, acetonitrile to 0.3% phosphoric acid solution) was pumped

18 up at 1 mL/min for 15 min. RES and PIP were detected at 306 and 342 nm, respectively.

19 The retention time of RES and PIP were 3.5 min and 12.6 min, respectively. The

20 calibration curves were linear over a range of 0.23-120.0 μg/mL for RES and 0.89-

21 56.75 μg/mL for PIP, with the correlation coefficients of around 0.999.

22

3. DSC analysis
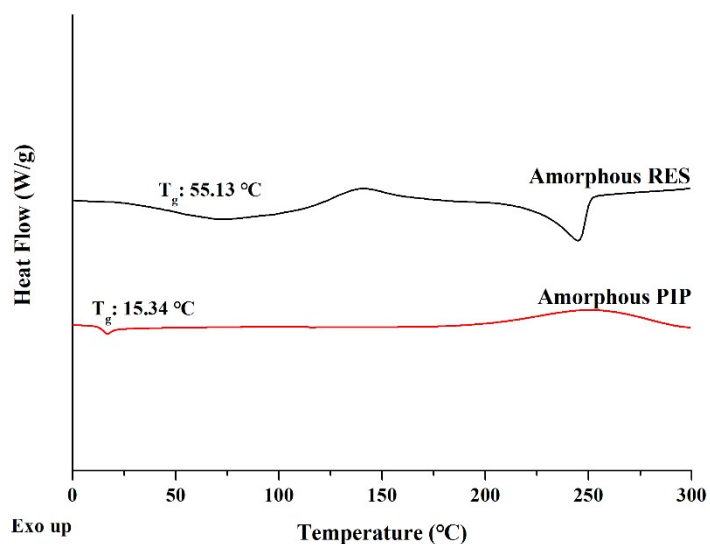
**Fig. S4** DSC thermograms of amorphous RES and amorphous PIP prepared *in situ* using differential scanning calorimetry.

Table S2 The predicted and experimental T_g of the RES-PIP CM system.

| Sample	Weight fraction	Experimental Tg, °C	Calculated Tg, °C	ΔT_g, °C
Amorphous RES	0.21	55.13	/	/
Amorphous PIP	0.79	15.34	/	/
RES-PIP CM	/	32.66	18.08	14.58

4. Crystal structure solution and refinement

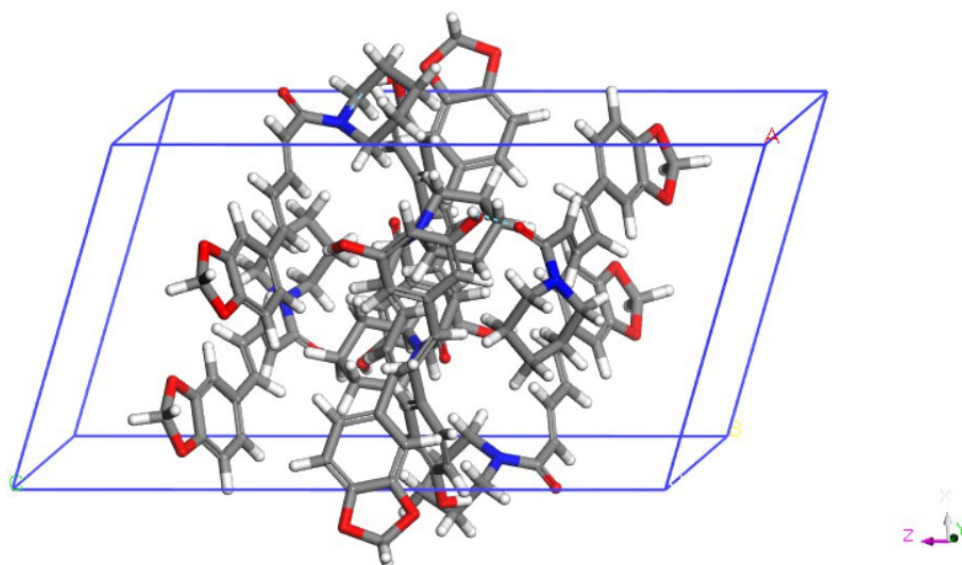Powder Refinement: Rwp = 7.96%   Rwp(w/o bck) = 7.47%   Rp = 9.43%
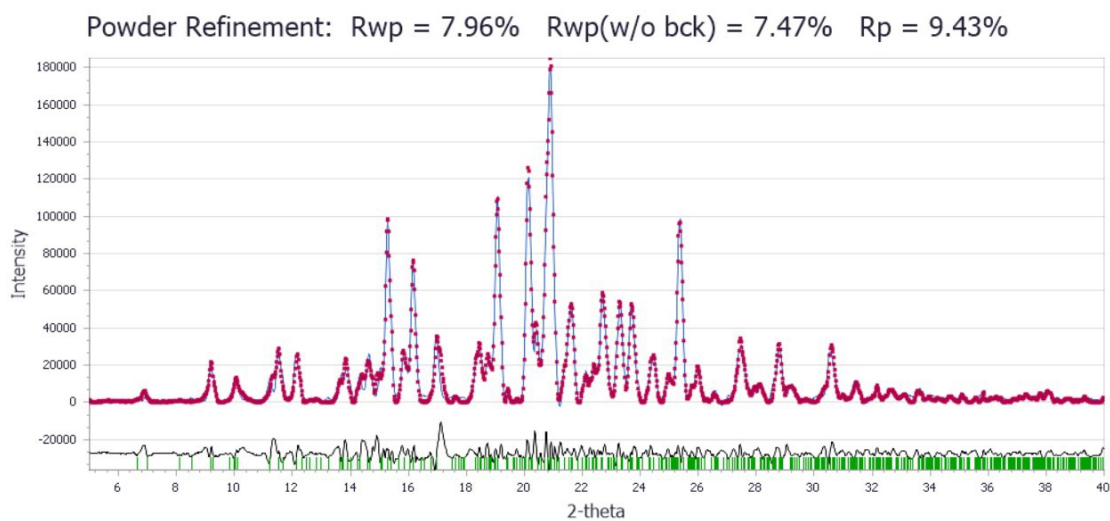
Fig. S5 The measured X-ray powder diffraction patterns (blue), Rietveld refinements (red) and underneath the difference curves (black) of RES-PIP CC. The green tick marks indicated reflection positions.
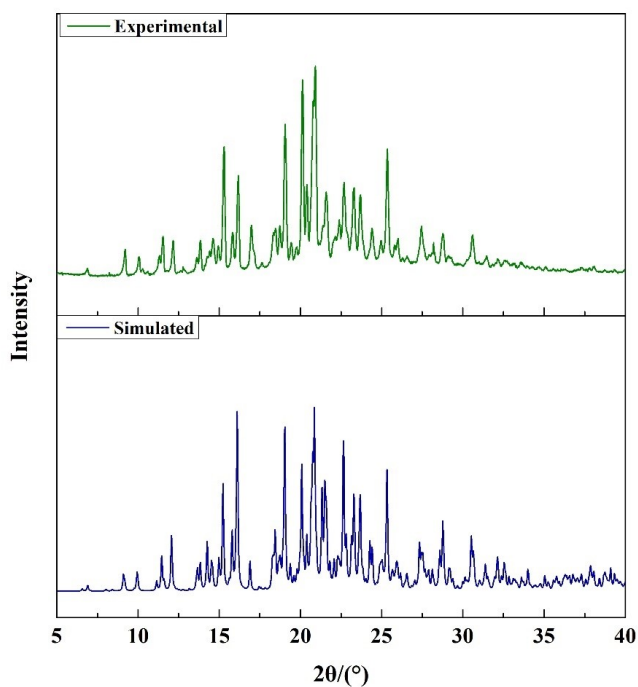
Fig. S6 Comparison of experimental and simulated patterns of RES-PIP CC.

39

40 **Fig. S7** The simulated structure of RES-PIP CC.

41

42 **Table S3** Crystallographic data of RES-PIP CC.

Parameters	RES-PIP CC
Formula	$(C_{14}H_{12}O_3)\cdot 3(C_{17}H_{19}NO_3)$
Space group	$P\bar{1}$
Crystal system	Triclinic
a(Å)	14.2960
b(Å)	10.0719
c(Å)	23.7853
α(°)	84.8598
β(°)	112.3810
γ(°)	105.4870
Volume (Å^3)	3051.56
R_{wp}%	7.96%

43

44 **Table S4** Hydrogen bond parameters for RES-PIP CC.

D-H···A	D···A/Å	H···A/Å	D-H···A/º
O7-H (RES)···O15 (PIP)	2.987	2.378	121.831
O17-H (RES)···N16 (PIP)	2.825	2.047	138.243

5. Polarizing light microscopy (PLM) and scanning electron microscopy (SEM)

Methods

5.1. PLM

A small amount of sample including crystalline RES, crystalline PIP, RES-PIP CM and RES-PIP CC was placed on a glass slide and dispersed with liquid paraffin. The surface morphology and birefringence phenomenon were observed and recorded by PLM (Eclipse Ci-POL, Nikon Ltd., Tokyo, Japan) under 10×20 times magnification.

5.2. SEM

The surface morphology of crystalline RES, crystalline PIP, RES-PIP CM and RES-PIP CC was observed by a SEM system (GeminiSEM 360, ZEISS Ltd., Jena, Germany). The sample was coated with a thin layer of gold and fixed on an SEM stub before observation. The SEM system was operated with probe current of 9400 nA, accelerating voltage of 3 kV, and counting time of 60 s, respectively. Furthermore, the gel formed from RES-PIP CM was also inspected by SEM to obtain its surface structure.

Results and discussion

PLM observation was conducted to analyze the morphology and birefringence behavior of the samples. Crystalline RES and crystalline PIP exhibited long flake state and irregular sphericity with obvious crystal birefringence, respectively (Fig. S8A & B). In contrast, the RES-PIP CM showed irregular block shapes without the birefringence phenomenon, indicating a complete amorphousness (Fig. S8C). While, RES-PIP CC appeared a regular long block or flake and visual crystal birefringence (Fig. S8D).

67 Furthermore, SEM was further applied to detect particle morphology after co-

68 amorphization and co-crystallization. Similar to PLM observation, the micrograph of

69 crystalline RES showed a long flake or columnar-like crystal shape (Fig. S8E), and

70 crystalline PIP exhibited an ellipsoid or spherical state with rough surface (Fig. S8F).

71 However, RES-PIP CM displayed irregularly lumpy or granular shapes after co-

72 amorphization (Fig. S8G). For RES-PIP CC, it showed a regular long block shape after

73 co-crystallization (Fig. S8H).
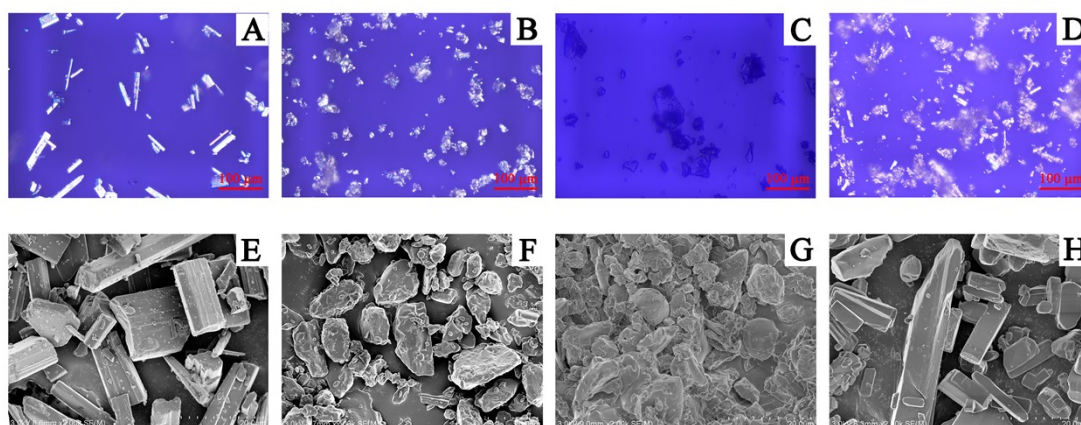
74

75 **Fig. S8** PLM and SEM images of (A, E) crystalline RES, (B, F) crystalline PIP, (C, G)

76 RES-PIP CM and (D, H) RES-PIP CC.

6. Ss ^{13}C NMR analysis

Table S5 Resonance assignments of RES and PIP in ^{13}C NMR spectra in solid state.

| Compound	Carbon Number	Chemical shift (ppm)
RES	1, 3	156.10
	14	154.07
	5	138.93
	12, 16	133.40
	11	129.30
	9, 10	125.40
	13, 15	117.47
	4, 6	110.62
	2	102.70
PIP	14	164.01
	4, 5	148.86
	12	142.00
	10	135.98
	7	131.33
	11	125.62
	8, 13	119.59
	9	107.30
	6	104.82
	2	102.88
	17, 21	43.87
	18, 19, 20	25.73

7. Transformation from RES-PIP CM to RES-PIP CC
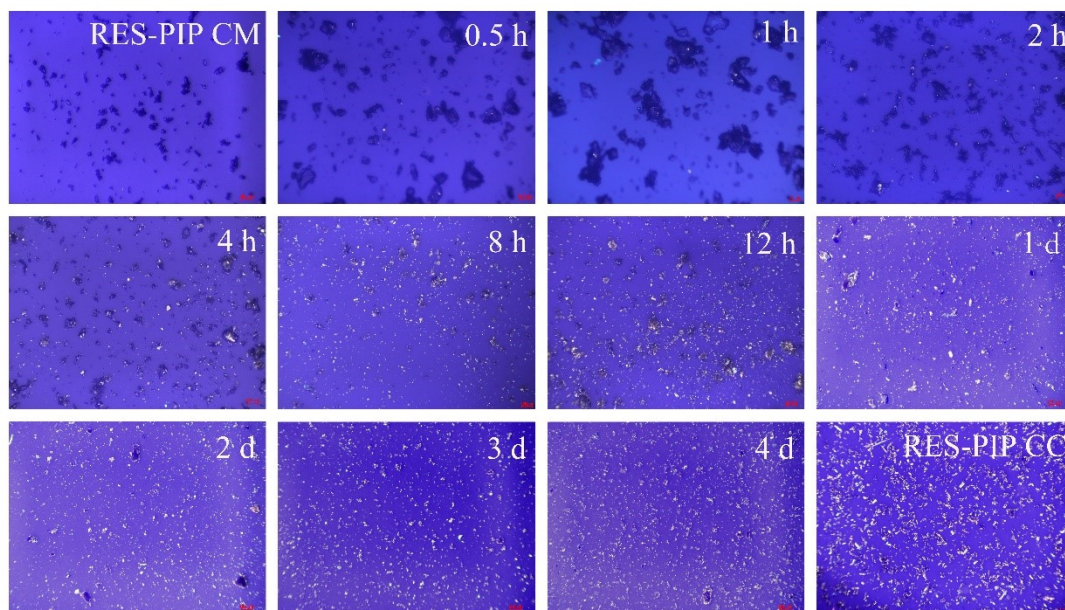
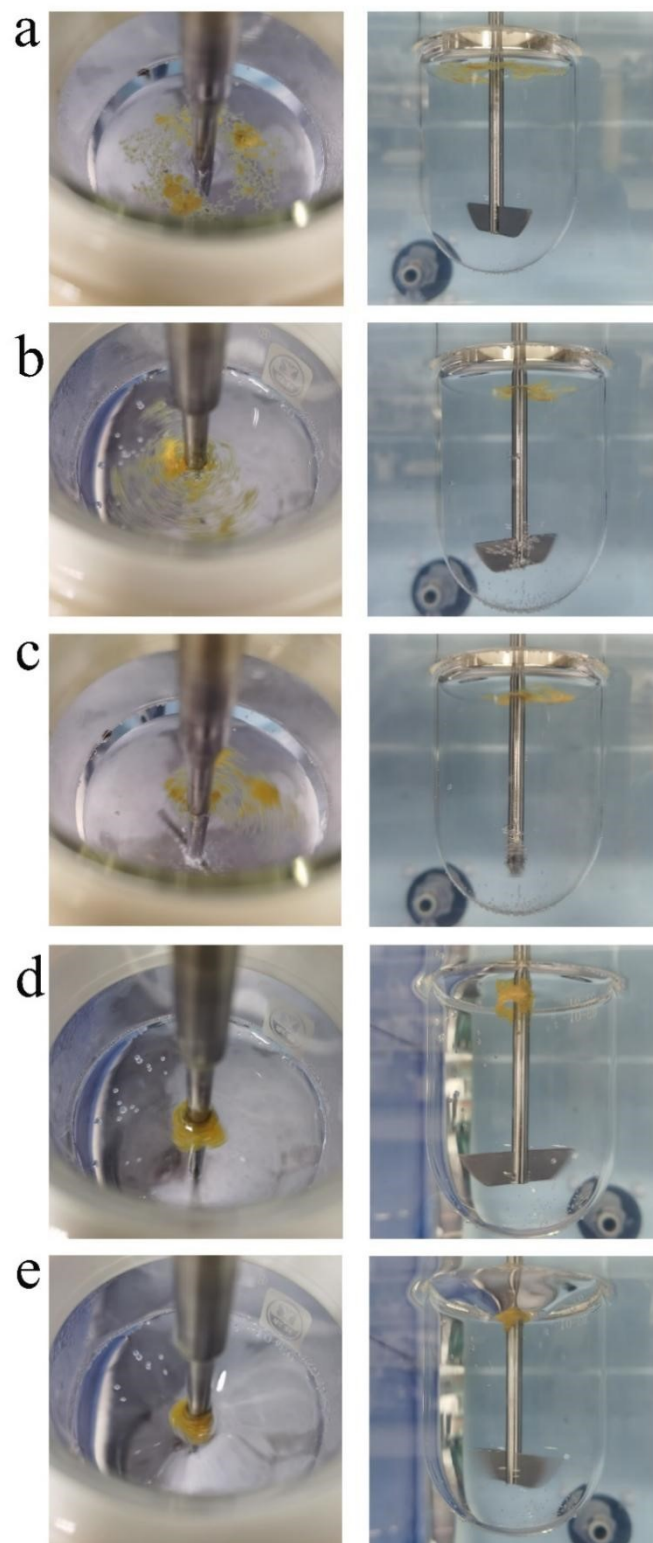**Fig. S9** PLM photographs of samples collected during dissolution of RES-PIP CM at different time.
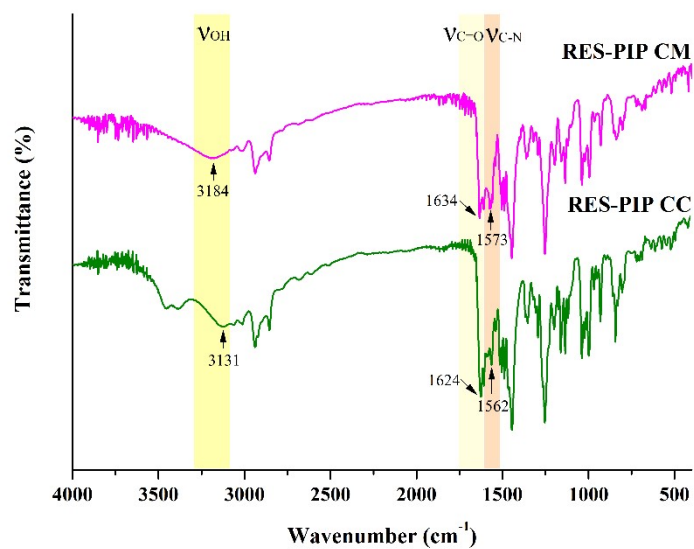
Fig. S10 FTIR spectra of RES-PIP CM and RES-PIP CC.

Fig. S11 Dissolution phenomena of RES-PIP CM at (a) 25, (b) 50, (c)100, (d) 150 and (e) 200 rpm.

8. Binding energy calculation between components

Methods

Molecular dynamics (MD) simulation was used to calculate the binding energy (E_{bind}) between components (including RES/RES, PIP/PIP and RES/PIIP) and further explore such transformation mechanism. E_{bind} is defined as the intermolecular interaction energy between different components. E_{bind} obtained from MD simulation has been widely used to evaluate the interaction of components, especially in the field of co-crystal explosives.[1-5]

The geometric structures of RES molecule and PIP molecule were optimized by Forcite module with the COMPASS II force field using Materials Studio software (version 2019, BIOVIA) to achieve the minimized energy structures.[6, 7] Amorphous cells of RES and PIP were established based on the molar ratios of RES-PIP CM and their respective densities (1.410 g/cm^3 for RES and 1.303 g/cm^3 for PIP) from Cambridge Crystallographic Data Centre. Next, the layered model of RES/PIP was built using RES amorphous cell as the first layer and PIP amorphous cell as the second layer. Similarly, the layered models of RES/RES and PIP/PIP were also established based on their respective amorphous cells. After the layered models were optimized to minimize the energy, COMPASS II force field and NPT ensemble were selected for MD simulation, and Andersen thermostat was selected for the temperature control. Meanwhile, the van der Waals force was simulated according to the Atom Based method, and the Electrostatic process is calculated with Ewald.[3, 6-8] The total simulation time was 200 ps and the time step was 1 fs. The temperature was set as 298 K, 310 K

114 and 318 K, respectively. Finally, the equilibrium layered structures of RES/PIP,

115 RES/RES and PIP/PIP at different temperatures could be obtained to calculate the E_{bind}

116 between components.

117   The E_{bind} was depicted as follows, and the greater the E_{bind}, the stronger the

118 interaction of components.[6-8]

119 $$E_{bind} = -E_{inter} = -\left[E_{total} - \left(E_{layer(1)} + E_{layer(2)}\right)\right]$$

120 Where E_{bind} is the binding energy of system, E_{inter} is the interaction energy between

121 molecules, E_{total} is the total energy of the whole equilibrium structure, $E_{layer(1)}$ and

122 $E_{layer(2)}$ represent the total energy of the first layer and the second layer, respectively.

123

124 **Results and discussion**

125 MD simulation was conducted to study the dynamic parameters and structural

126 properties of the RES-PIP system, in order to explore the transformation mechanism

127 from RES-PIP CM to RES-PIP CC. The stable structure is formed by the strong

128 intermolecular interactions (especially intermolecular hydrogen bonds) between

129 components in co-amorphous system. The MD methods were used to build the

130 amorphous cell models of RES and PIP (Fig. S12), the layered models of RES/RES,

131 PIP/PIP and RES/PIP were constructed using RES amorphous cell and PIP amorphous

132 cell (Fig. S13), and the layered structures were optimized and run by MD simulation at

133 different temperatures to obtain the equilibrium structures (Fig. S14-S16). On this basis,

134 the binding energy (E_{bind}) of RES/RES, PIP/PIP and RES/PIP was calculated in Table

135 S6. The E_{bind} reflects the strength of intermolecular interactions between components.[6-8]

136 The greater E_{bind} means the stronger interactions and the more stable internal structure

137 of the system. According to the analysis of MD simulation, the E_{bind} between RES and

138 PIP in the RES-PIP CM system at 298 K, 310 K and 318 K was approximately 1190

139 kcal/mol, 1124 kcal/mol and 1093 kcal/mol, respectively, which were significantly

140 greater ($p < 0.01$) than those between the single components (i.e., RES/RES, PIP/PIP),

141 indicating that the strongest intermolecular interactions between RES and PIP than
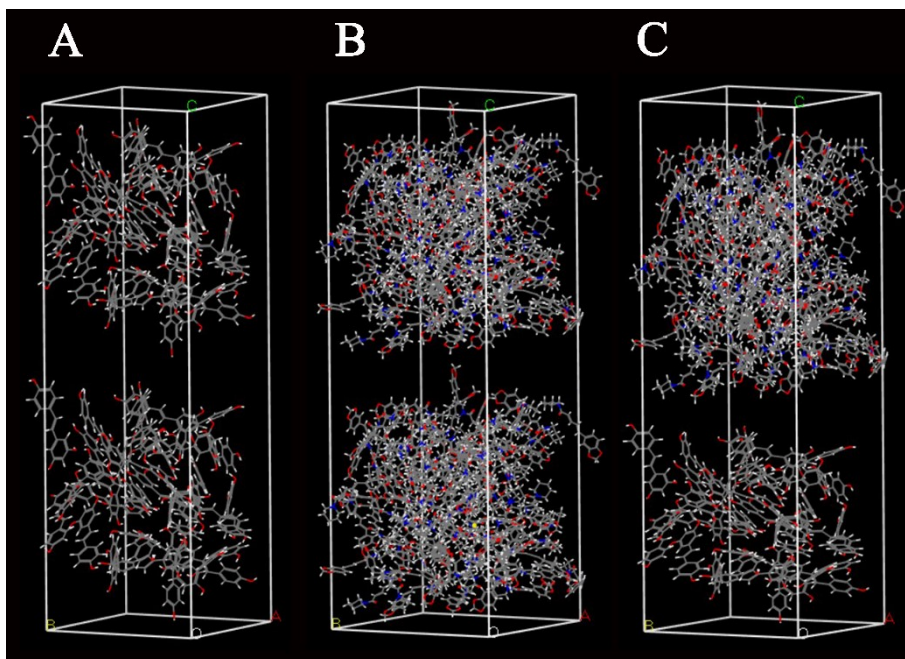
142 those of the same components.

143
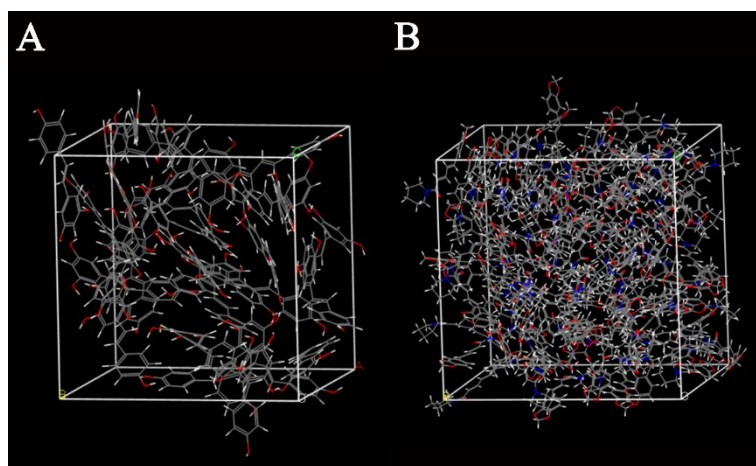
144

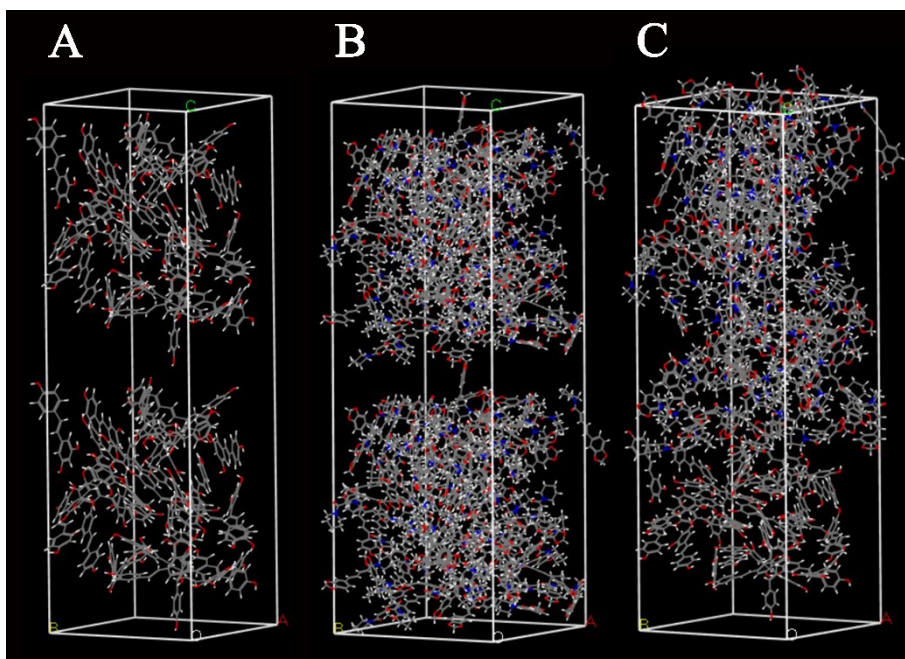145 **Fig. S12** Amorphous cells of (A) RES molecules and (B) PIP molecules.

146

147

Fig. S13 The initial layered structures of (A) RES/RES, (B) PIP/PIP and (C) RES/PIP
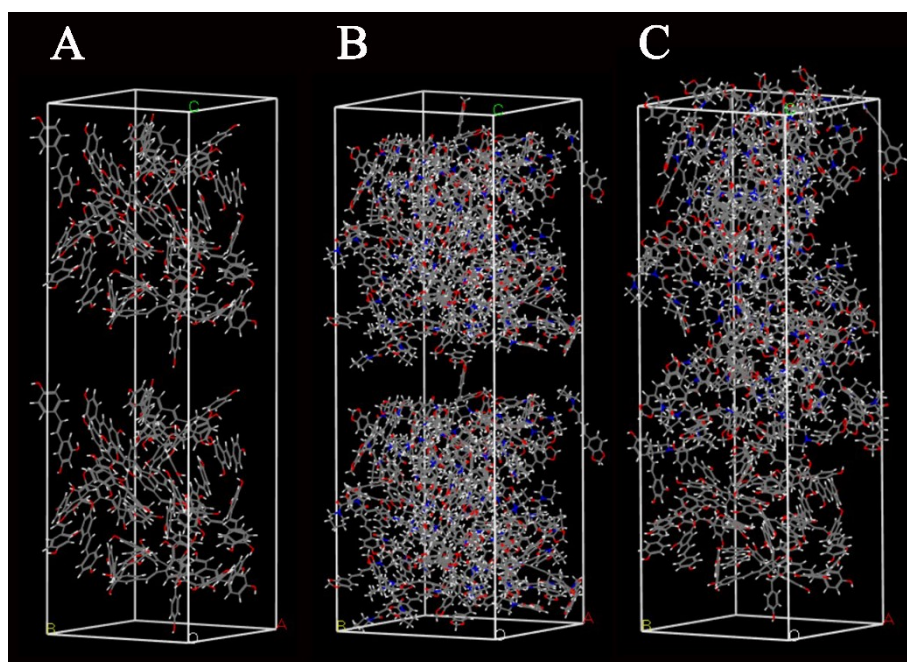
built by amorphous cells.

150

151

Fig. S14 Equilibrium layered structures of (A) RES/RES, (B) PIP/PIP and (C) RES/PIP

at 298 K.
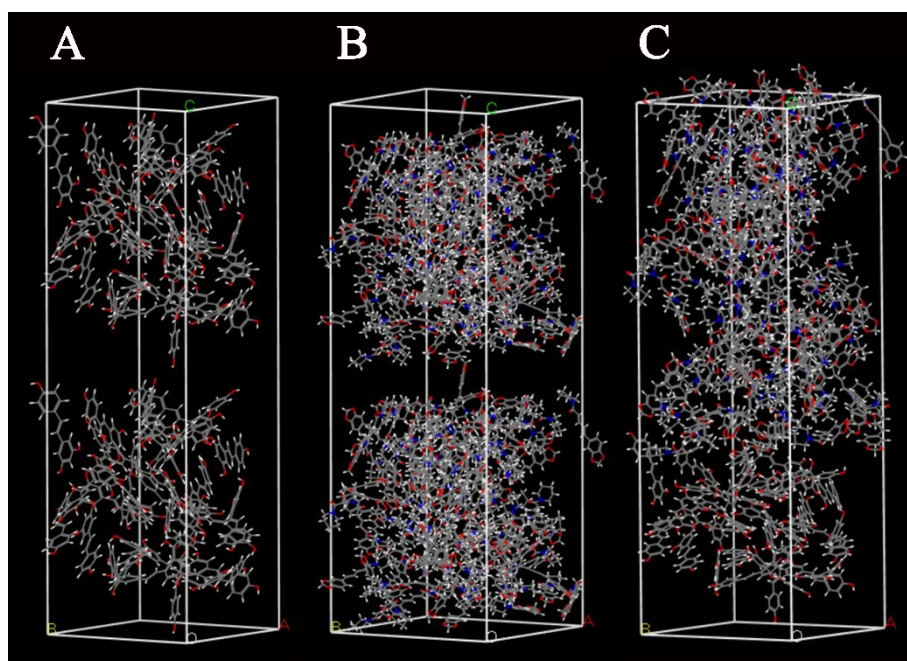
154

155

Fig. S15 Equilibrium layered structures of (A) RES/RES, (B) PIP/PIP and (C) RES/PIP

at 310 K.

158

159

Fig. S16 Equilibrium layered structures of (A) RES/RES, (B) PIP/PIP and (C) RES/PIP

at 318 K.

162

163

164 **Table S6** Binding energy (E_{bind}) between components in the RES-PIP CM system at

165 different temperatures.

Temperature	Sample	Total energy/(kcal/mol)	Layer (1)/(kcal/mol)	Layer (2)/(kcal/mol)	E_{bind}/(kcal/mol)
298 K	RES/RES	-1295.560	-587.151	-602.357	106.052
	PIP/PIP	7344.348	3714.363	3741.760	111.775
	RES/PIP	3073.013	-417.476	4680.588	1190.099[**##]
310 K	RES/RES	-1123.203	-528.525	-522.126	72.552
	PIP/PIP	7767.039	3983.376	4003.341	219.678
	RES/PIP	3375.837	-337.898	4837.386	1123.651[**##]
318 K	RES/RES	-1070.777	-493.796	-491.618	85.363
	PIP/PIP	8055.663	4183.959	4150.548	278.844
	RES/PIP	3549.504	-299.958	4942.671	1093.209[**##]

166 $^{*}p < 0.05$, $^{**}p < 0.01$, compared to RES/RES. $^{\#}p < 0.05$, $^{\#\#}p < 0.01$, compared to PIP/PIP.

167
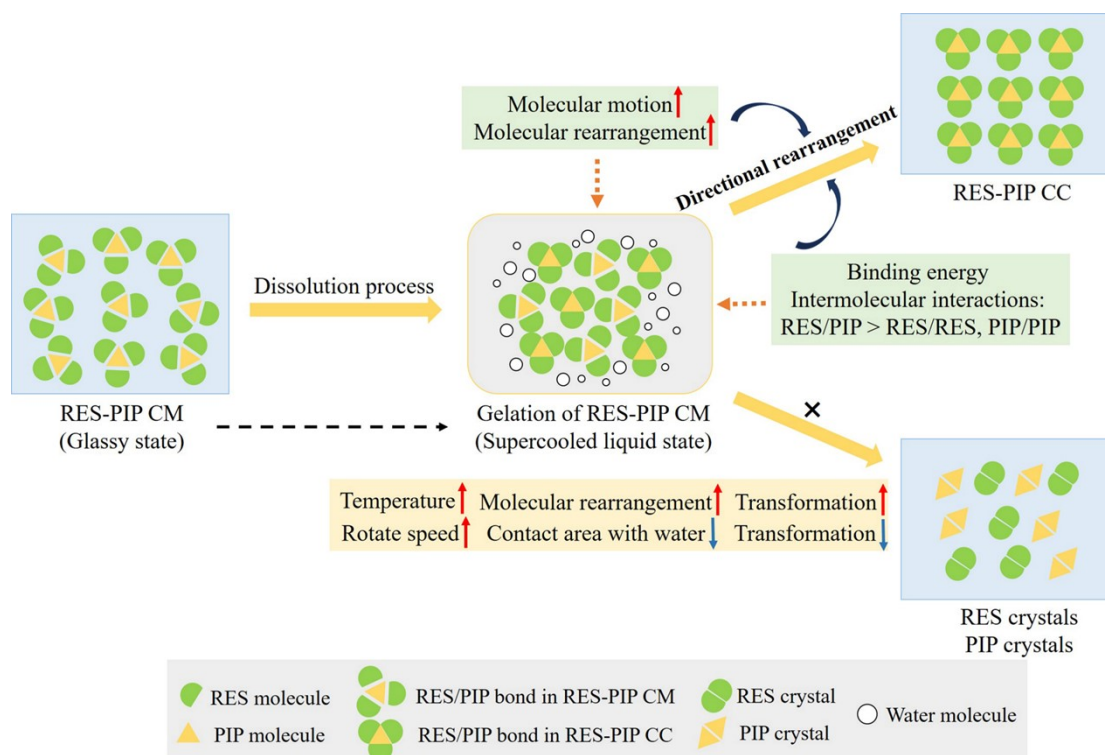
168

169 **Fig. S17** Proposed schematic diagram of transformation from RES-PIP CM to RES-

170 PIP CC during dissolution process.

References

1. B. H. Duan, Y. J. Shu, N. Liu, Y. Y. Lu, B. Z. Wang, X. M. Lu and J. Q. Zhang, *Rsc Adv.*, 2018, **8**, 34690-34698.

2. G. Y. Hang, J. T. Wang, T. Wang, H. M. Shen, W. L. Yu and R. Q. Shen, *J. Mol. Model.*, 2022, **28**, 58.

3. G. Y. Hang, W. L. Yu, T. Wang and J. T. Wang, *J. Mol. Model.*, 2019, **25**, 10.

4. G. Y. Hang, W. L. Yu, T. Wang, J. T. Wang and Z. Li, *J. Mol. Struct.*, 2017, **1141**, 577-583.

5. X. Zhao, X. Fu, G. Zhang, X. Liu and X. Fan, *ACS omega*, 2022, **7**, 7361-7369.

6. X. J. Wang and J. J. Xiao, *Struct. Chem.*, 2017, **28**, 1645-1651.

7. S. L. Xiong, S. S. Chen, S. H. Jin, Z. Zhang, Y. Zhang and L. J. Li, *Rsc Adv.*, 2017, **7**, 6795-6799.

8. K. P. Song, F. D. Ren, S. H. Zhang and W. J. Shi, *J. Mol. Model.*, 2016, **22**, 249.